American Mineralogist, Volume 68, pages 0–0, 1983

An electron microscope study of leucophoenicite

TIMOTHY J. WHITE[1] AND BRUCE G. HYDE

Research School of Chemistry, Australian National University
P.O. Box 4, Canberra, A.C.T. 2600, Australia

Abstract

Three leucophoenicite specimens were examined in the transmission electron microscope and by X-ray powder diffraction and electron-probe microanalysis. A comparison of observed and computer-simulated structure images supports Moore's proposals that the leucophoenicite structure possesses edge-shared pairs of O_4 tetrahedra that are half-occupied by Si, and that the crystals contain planar faults parallel to (001). The latter are interpreted as lamellae of other members of a proposed leucophoenicite series (analogous to the well-known humite series). Such faults frequently cause microtwinning, often on a scale of less than 100Å. Humite series members were also very occasionally intergrown with leucophoenicite, and one specimen (from Pajsberg, Sweden) was associated with chrysotile. In the electron beam leucophoenicite readily decomposes to tephroite, Mn_2SiO_4.

Introduction

Leucophoenicite is dimorphic with manganhumite, ideally $3Mn_2SiO_4 \cdot Mn(OH)_2$, although the former always contains several weight percent of CaO (in the present specimens ~6%). A morphological study by Palache (1928) indicated that it is crystallographically distinct from the humite minerals, and a preliminary power X-ray examination (Moore, 1967) suggested the existence of several leucophoenicite types with monoclinic or orthorhombic symmetry. Finally, a single crystal X-ray structure analysis by Moore (1970) showed that leucophoenicite is monoclinic $P2_1/a$, with the crystallochemical formula $Mn_7[SiO_4]_2[(SiO_4)(OH)_2]$. We have reoriented to $P2_1/b$, a-axis unique in order to facilitate a direct comparison with the structures of the humite minerals (*Pbnm* or $P2_1/b$) and olivine (*Pbnm*).

However, following Moore's studies many incompletely identified specimens remained; in particular the question of orthorhombic polymorphs was not settled (see also Cook, 1969).

Structural considerations

Moore (1970) described leucophoenicite as a hexagonally-close-packed (h.c.p.) anion array with the larger cations (mainly Mn) in octahedral interstices and the smaller (Si) in tetrahedral interstices. We have previously proposed an alternative description in which anions are inserted into the interstices of a cation array, which is rather more regular than the anion array and corresponds to a simple alloy structure (White and Hyde, 1983a). The cation array is twinned, cubic-close-packed (c.c.p.) Mn with Si in three-quarters of the Mn_6 trigonal prisms at the composition planes. Two protons occupy each of the remaining prisms. Oxygen atoms are in $SiMn_3$ tetrahedra and Mn_3 triangles (HMn_3 tetrahedra).

The cation array is a regular intergrowth of the **Ni_2In** alloy type (twinned c.c.p. Ni . . . 2,2 . . . with In in Ni_6 trigonal prisms) and the **CrB** alloy type (twinned c.c.p. Cr . . . 1,1 . . . with B in Cr_6 trigonal prisms) (Hyde *et al.*, 1979). Thus, leucophoenicite is twinned c.c.p. Mn . . . 1,2,2,2,1,2,2,2 . . . or $(1,2^3)$ with Si or 2H in each of the Mn_6 trigonal prisms. The twin bands are one or two atoms wide. This approach yields simple relations between the structures of a proposed leucophoenicite family and those of the humite family and olivine. Figure 1 shows leucophoenicite in both descriptions. Here we concentrate on the cation array.

Electron microscopy

Three leucophoenicite specimens were examined; details are given in Table 1. For examination in the transmission electron microscope, fragments were ground under ethanol in an agate mortar and then mounted on holey-carbon films supported on copper grids. They were studied at 100 kV in a JEOL 100CX microscope fitted with a high-resolution, side-entry stage or at 200 kV in a JEOL 200CX microscope with an ultra-high-resolution, top-entry stage. Both instruments had standard hair-pin filaments. Correction of objective-lens astigmatism was carried out on the carbon support film by minimizing contrast. High-resolution images were recorded at magni-

[1]Present Address: School of Science, Griffith University, Brisbane, Queensland 4111, Australia

Table 1: Leucophoenicite specimens used in the study

Prefixes for Museum Numbers:

BM British Museum of Natural History
SI Smithsonian Institute (Natural History)
SM Swedish Museum of Natural History

Sample and Source	Constituents Found	Observations
Franklin Mine, Sussex County, N.J., U.S.A. (BM 1946, 185)	$(1,2^3)$ leucophoenicite, + a little tephroite (2^2) and sonolite $(2^3,3)$.	Almost all crystals showed a considerable degree of faulting. Approximately half were twinned microscopically (i.e. twin bands < 100 Å wide).
Franklin Mine, Sussex County, N.J., U.S.A. (SI C6800)	$(1,2^3)$ leucophoenicite	Most crystals were "perfect". Two fragments were heavily faulted, and one fragment exhibited twinning.
Pajsberg, Sweden (SM 740214)	$(1,2^3)$ leucophoenicite, + a little manganhumite $(2^2,3)$ + some orthochrysotile	The $(1,2^3)$ leucophoenicite was mainly perfect; two crystals were twinned microscopically. The orthochrysotile was intergrown with another phase, possibly talc.

fications of 380,000×, 550,000× or 810,000×. Linear imaging conditions (*i.e.*, crystals less than 80Å thick) were always utilized.

Cleavage normal to [100] (the principal zone of interest) was well defined, and large thin crystals were abundant. Beam damage was severe and rapid, particularly for heavily-faulted crystals.

Image interpretation

Images from the 100CX instrument consisted of (001) fringes. The 200CX yielded higher-resolution lattice images and structure images which could be matched with computer-simulated images. The program used for the image calculations was purchased from Arizona State

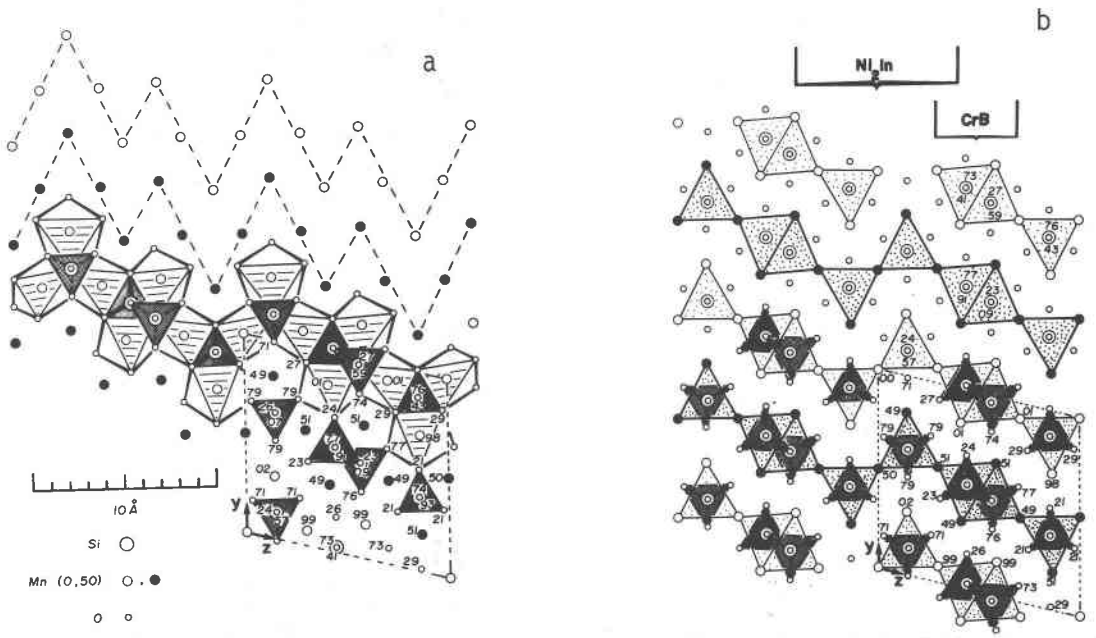

Fig. 1. Moore's (1979) structure of leucophoenicite projected on (100). a. Structure in conventional terms: h.c.p. anions with cations in octahedral and tetrahedral sites. Also emphasized are sheets of twinned c.c.p. cations, the repeat unit consisting of one band one atom wide (1) followed by three bands two atoms wide (2), which leads to the twin formula $(1, 2^3)$. b. Structure emphasizing the alloy-type structure of the cation array. (Note that this is more regular than the anion array above). Rows of edge-connected $SiMn_6$ trigonal prisms are of the **Ni_2In** type; the pairs of face-sharing trigonal prisms are of the **CrB** type. In the proposed leucophoenicite series various widths of the **Ni_2In** type are inserted between **CrB**-like elements. (The olivine structure is anion-stuffed **Ni_2In**, with no **CrB**-like layers.)

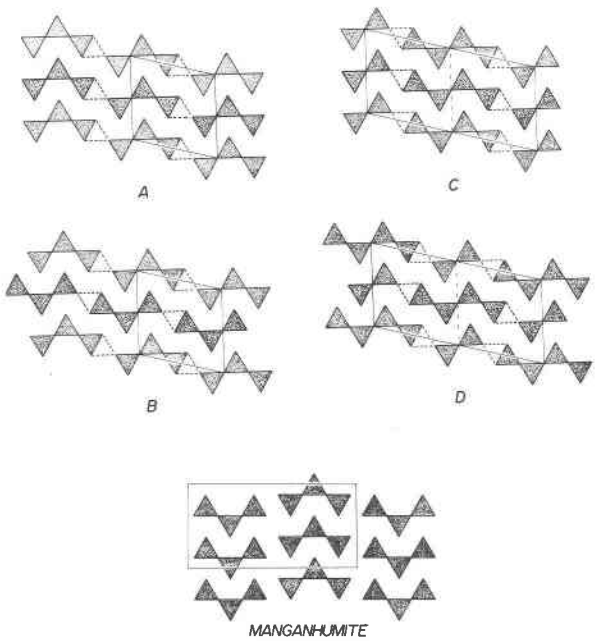

Fig. 2. Ordering of the Si atoms in (1, 2^3) leucophoenicite can produce many polymorphs. The four simplest, designated A, B, C, and D, are shown projected down [100]. (Si-free Mn_6 trigonal prisms are outlined by dashes.) Note that the (1, 2^3) cation array is maintained. Manganhumite (2^2, 3)^2 is also shown.

University and adapted to run on the A.N.U. Univac computer by Dr. J. R. Sellar and Dr. R. A. Eggleton. The following instrumental parameters were employed for the image calculations: incident beam convergence = 0.2 or 0.4 mrad, objective aperture radius 0.39 or 0.79Å^{-1}, coefficient of spherical aberration, C_s = 1.5 mm, depth of gaussian focus = 150Å, slice thickness = 4Å.

Results

The distribution of Si atoms

Moore's (1970) determination of the leucophoenicite (1, 2^3) structure showed two crystallographically distinct Si atoms. The first SiO_4 tetrahedron (in our description the edge-sharing Mn_6Si trigonal prisms) is isolated and the Si site fully occupied. The second Si is statistically distributed between two tetrahedra of an edge-shared pair, *i.e.*, in an [$(SiO_4)(OH)_2$] group (or alternatively a pair of face-shared Mn_6 trigonal prisms).

If the latter Si arrangement is ordered a number of polymorphs are possible: four simple ones emphasizing the trigonal prism array are shown in Figure 2. Structure images were calculated for both [100] and [010] projections of Moore's statistical model and polymorphs A and B (Figs. 3 and 4). (The calculated images for polymorphs C and D are readily deduced by considering those of the other ordered polymorphs, particularly around the optimum defocus of −600Å.) A comparison of the calculated and experimental images (Figs. 5 and 6) supports the structure proposed by Moore, at least over the thicknesses studied.

Lamellar faults

As expected from Moore's earlier X-ray studies faults parallel to (001) were found, especially in one of the samples from Franklin, N.J. (BM 1946, 185). (The other samples were less imperfect.) A low-resolution lattice image of an inhomogeneous crystal is shown in Figure 7. High-resolution lattice images support the notion that the variations are very thin lamellae (one or two unit cells wide) of higher members of a leucophoenicite series, (1, 2^x) with $x > 3$ (Figs. 5 and 8). No lower members ($x < 3$) were observed.

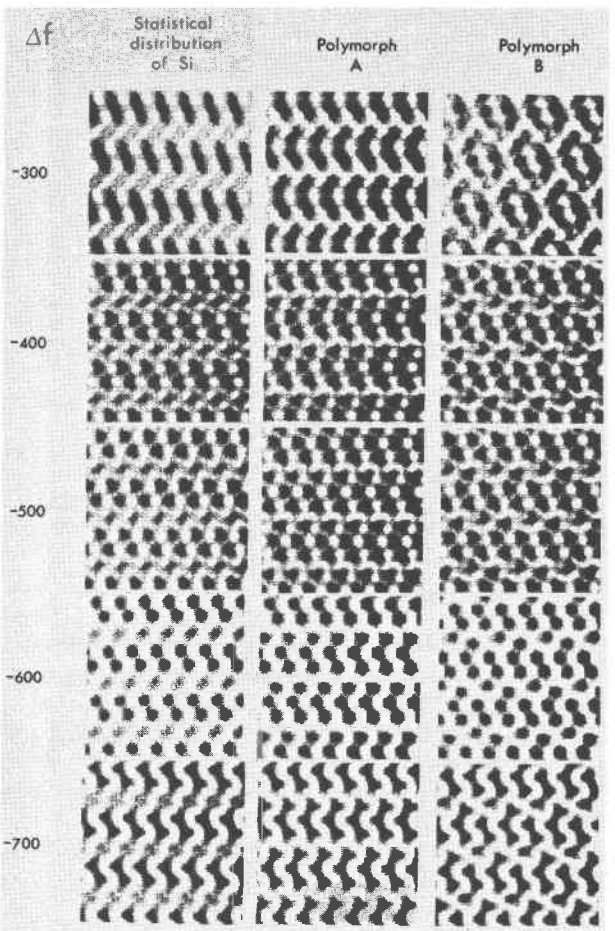

Fig. 3. Calculated through-focus series of images for the [100] zone using the statistical model of leucophoenicite, and also the ordered polymorphs A and B. (Computational parameters were: thickness = 40Å, objective aperture radius = 0.39Å^{-1}, C_s = 1.5Å, beam divergence = 0.2 mrad, chromatic abberation = 150Å, and defocus Δf = −300 to −700Å).

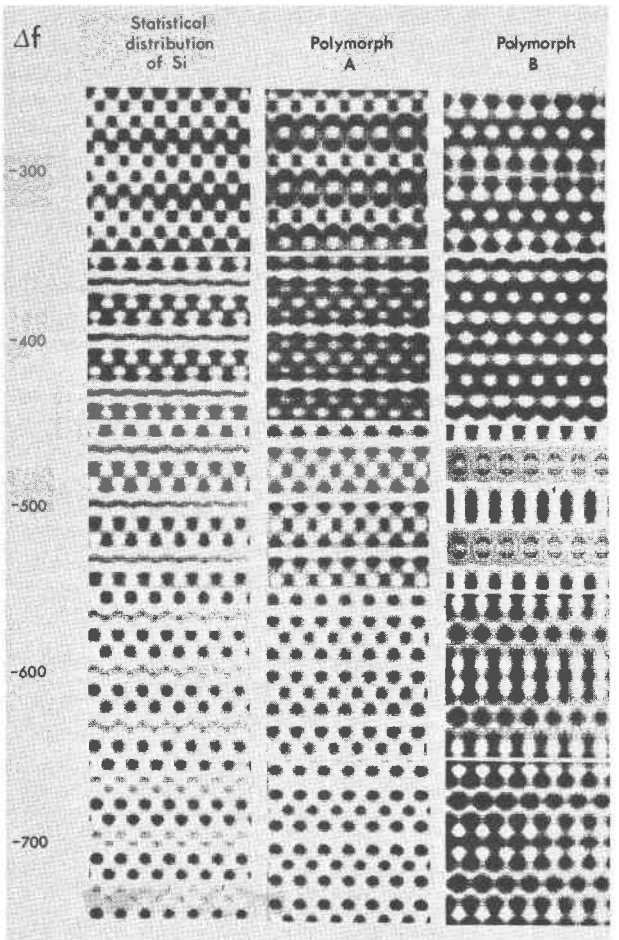

Fig. 4. Simulated computer images for the [010] zones for the statistical model of (1, 2^3) leucophoenicite and also for its two simplest ordered polymorphs. (Computational parameters are the same as for Fig. 3.)

Partly-ordered, long-range sequences were sometimes observed. An example is given in Figure 9 where (mostly) ($1,2^5$) elements are dispersed in a ($1,2^3$) matrix. As well as simple intergrowths, more complex faults [not parallel to (001)] were also observed (Fig. 10). Higher-magnification images of the latter show that in some instances the lattice fringes either side of the fault appear to have reversed contrast (Fig. 11A) suggesting a twin relation across the fault surface (*cf.* below), while in other cases (Fig. 11B) interpretation is impossible because of changes in contrast which may be due to strain fields. The lattice image at either end of the fault then becomes very complex indeed. (See also Fig. 15*a*.) It seems likely that these faults are jogs connecting terminating faults of the common type [($1,2^x$) with anomalous x] on widely spaced (001) planes, but this hypothesis has not been adequately checked.

Microtwinning

The electron diffraction pattern of a twinned crystal contains reflections from both twins. For leucophoenicite crystals twinned on (001) the two sets of reflections will superimpose (almost exactly) in $[h\bar{1}0]$ zones with h even. For $[h\bar{1}0]$ zones with $h = 2n + 1$ the reflections in hkl rows with $k = 2n + 1$ will not superimpose. Thus a series of $[h\bar{1}0]$ diffraction patterns obtained by tilting about **c*** shows the alternation in appearance schematically illustrated in Figure 12.

Images from relatively thick regions (100–150Å) of twinned crystals showed bands of alternating contrast (Fig. 13, also Fig. 10). (This variation in contrast was never observed in untwinned crystals.) The "doubled rows" of spots in the diffraction patterns of twinned crystals were often not quite straight. This was even more apparent when the SAD patterns were defocussed; the two sets of reflections moved in opposite directions along **c***. This indicates two crystallographically distinct regions related by a 180° rotation about a twin axis (which in this case is parallel to [010] and perpendicular to the electron beam).

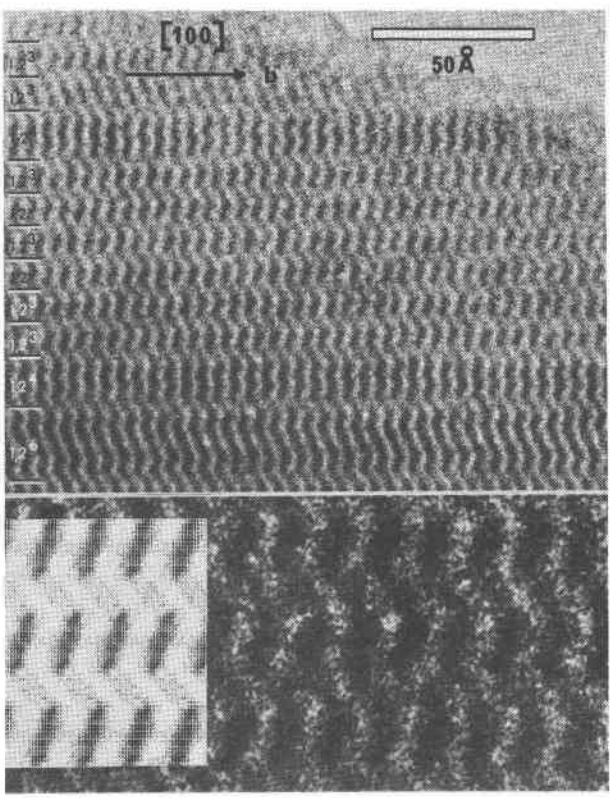

Fig. 5. A high-resolution structural image of leucophoenicite (BM 1946, 185). The calculated image most closely matching the micrograph is that obtained from Moore's statistical model (*cf.* Fig. 3). Note the intergrowth with higher members of the leucophoenicite series, (1, 2^4) and (1, 2^6).

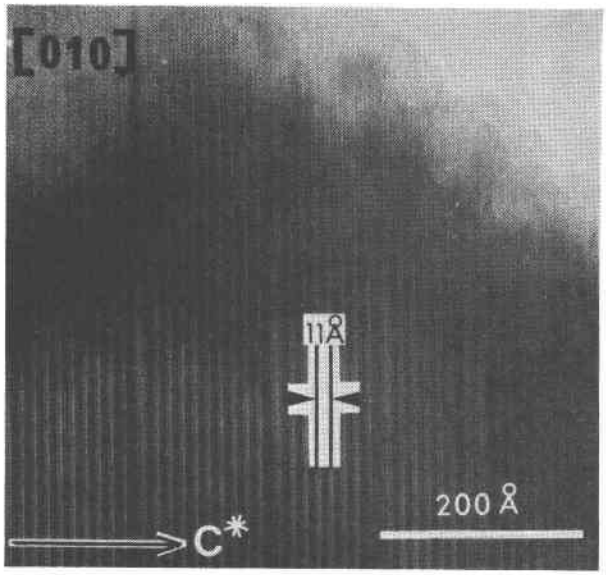

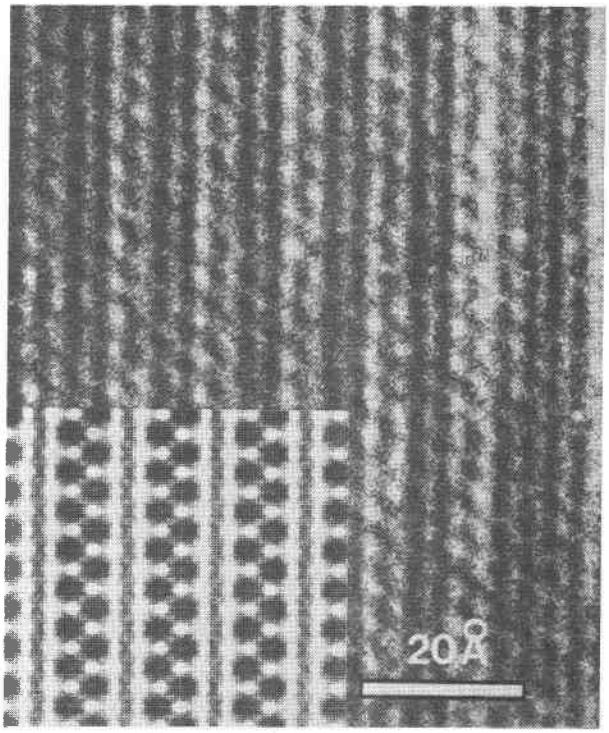

Fig. 6. A micrograph of (1, 2^3) leucophoenicite in the [010] zone. (BM 1946, 185). The most closely matching calculated image is obtained from Moore's statistical model for (1, 2^3) leucophoenicite (*cf.* Fig. 4).

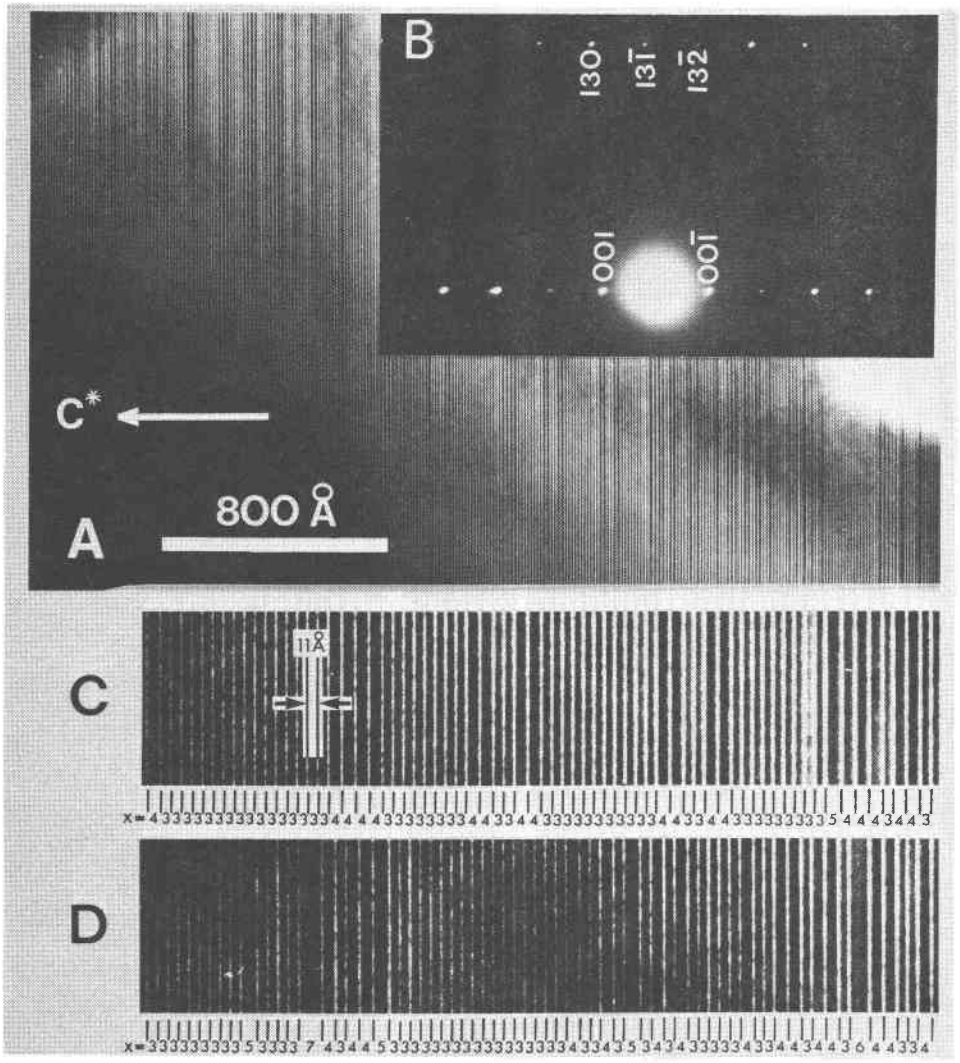

Fig. 7. An inhomogeneous region of a predominantly (1, 2^3) leucophoenicite crystal (BM 1946, 185). A. Low magnification image showing extensive disorder. B. Corresponding selected-area diffraction pattern: note the weak additional spots indicative of twinned leucophoenicite. C, D. Higher-magnification images interpreted as members of the proposed leucophoenicite-type series (1, 2^x).

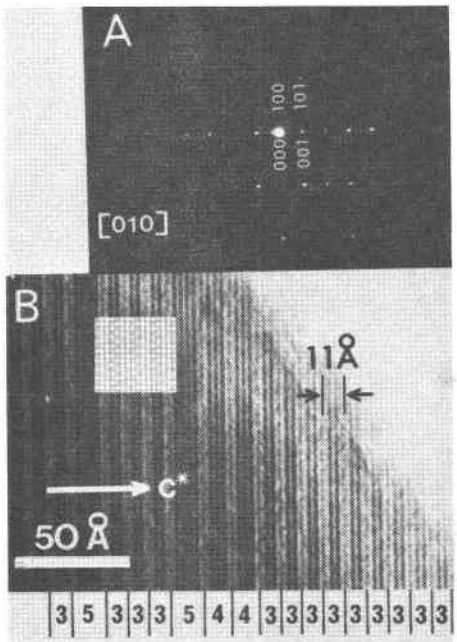

Fig. 8. A higher-resolution lattice image of leucophoenicite (BM 1946, 185). A. Selected area diffraction pattern. B. Coherent intergrowth between members of a "leucophoenicite series." Images were calculated only for (1, 2^3); however it is likely that darker bands are Ni_2In (olivine) lamellae and lighter bands are CrB lamellae.

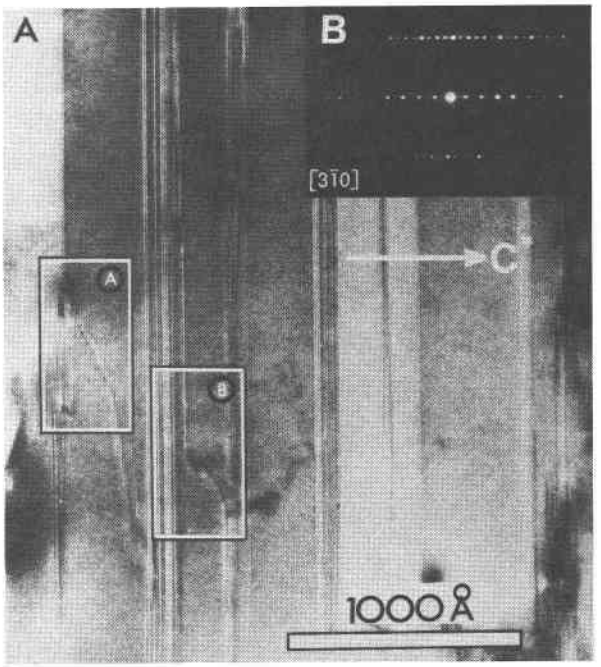

Fig. 10. A. A twinned (1, 2^3) leucophoenicite crystal (BM 1946, 185); note the light and dark bands indicative of the two twin orientations. The rectangles outline areas with faults not parallel to (001). B. Corresponding SAD pattern. The apparent $(22Å)^{-1}$ arises from twinning on (001).

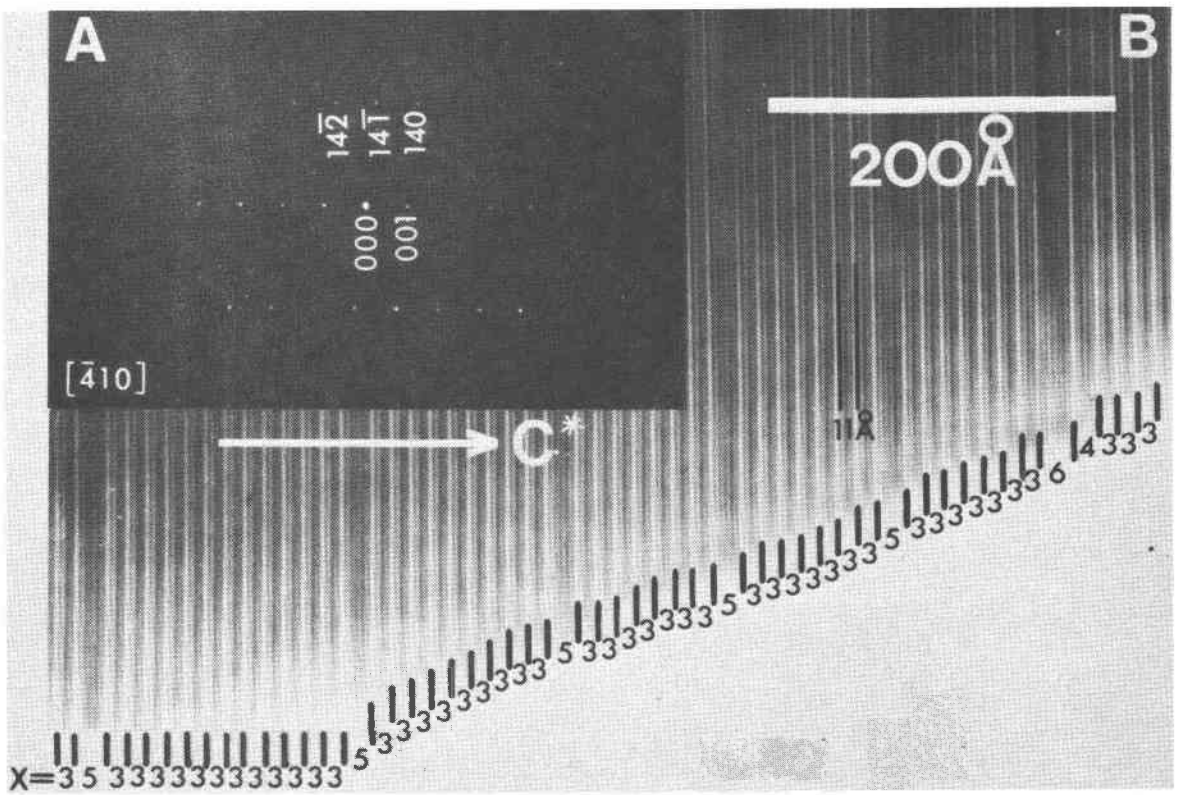

Fig. 9. A. Selected-area diffraction pattern. B. Corresponding high-resolution lattice image showing periodic insertion of a (1, 2^5) member in a matrix of (1, 2^3) (BM 1946, 185). (Notice that the number of faults is quite small if the parent structure is taken to be [1, 2^5,(1, 2^3)^7], a complex superstructure with $d(001) \simeq 185$Å.)

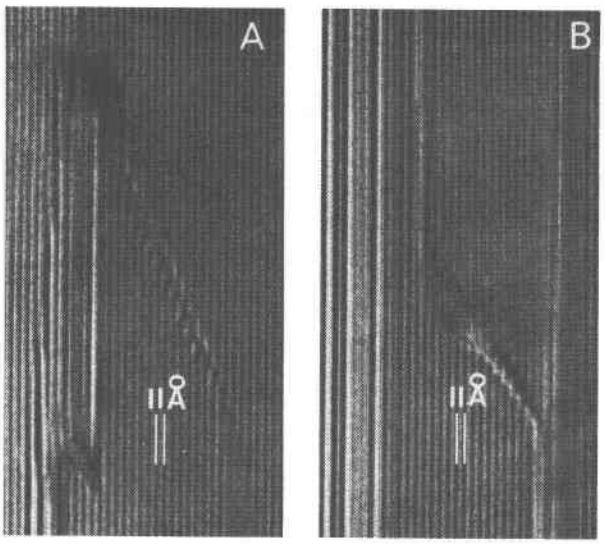

Fig. 11. Enlargements of areas A and B in Figure 10. A. Note the reversal of contrast in the main lattice fringes across the diagonal fault, suggesting twinning. B. Changes in contrast in the region above the diagonal fault makes interpretation difficult. Twinning dislocations (lateral shifts in unit-cell twin planes) are apparent in both cases; and perhaps also an edge dislocation in B.

Of course it is not surprising that twinned leucophoenicite crystals occur. Twin boundaries are readily introduced in $(1,2^3)$ leucophoenicite by intergrowth with an odd number of lamellae of any orthorhombic member of the proposed series $(1,2^x)$ with x even. An example of such a boundary is shown schematically in Figure 14.

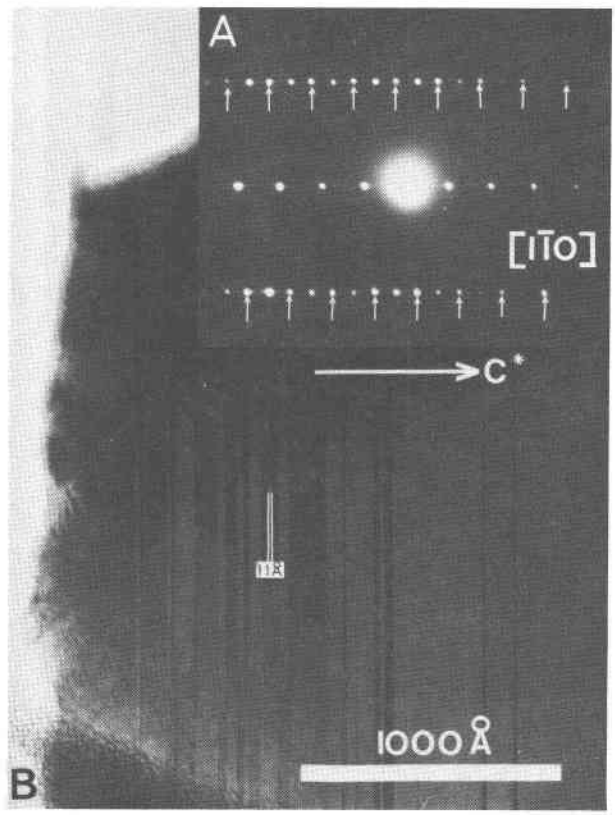

Fig. 13. A leucophoenicite crystal (repeatedly) twinned on (001) (BM 1946, 185). A. SAD pattern. The reflections belonging to one of the two twin orientations are distinguished by arrows. Note that the "doubled" rows of spots are not quite straight. B. Low-resolution image showing the alternating dark and light bands which were characteristic of twinned crystals.

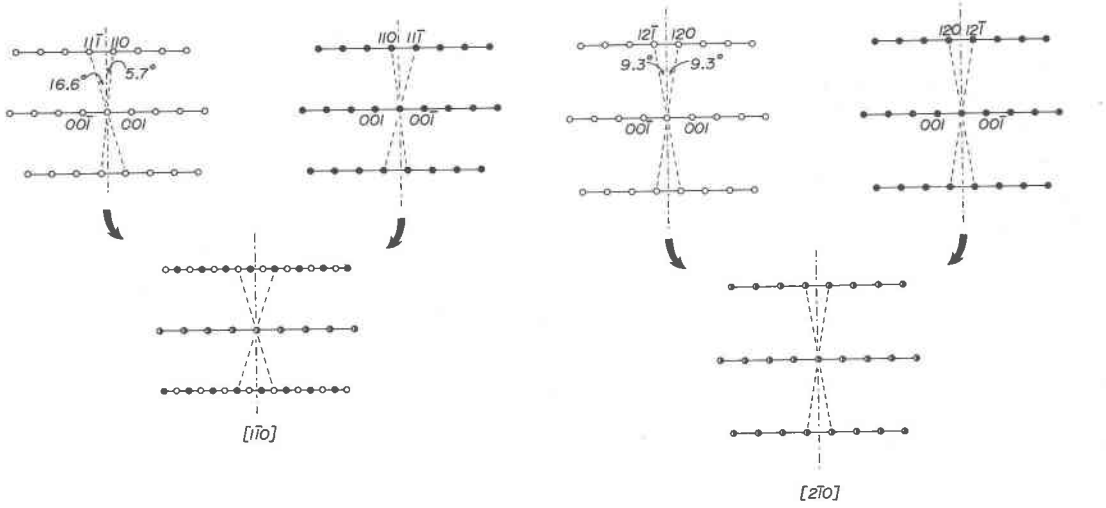

Fig. 12. Schematic illustration of the $[h\bar{1}0]$ zone axis diffraction patterns expected for leucophoenicite crystals twinned on (001): zone axes $[1\bar{1}0]$ and $[2\bar{1}0]$. The upper diagrams are for untwinned crystals, open and closed circles for twins I and II respectively. The lower diagrams are for twinned crystals, half-filled circles being superimposed reflections from both twins. Note the doubling of the number of reflections in alternate rows of the $[1\bar{1}0]$ zone.

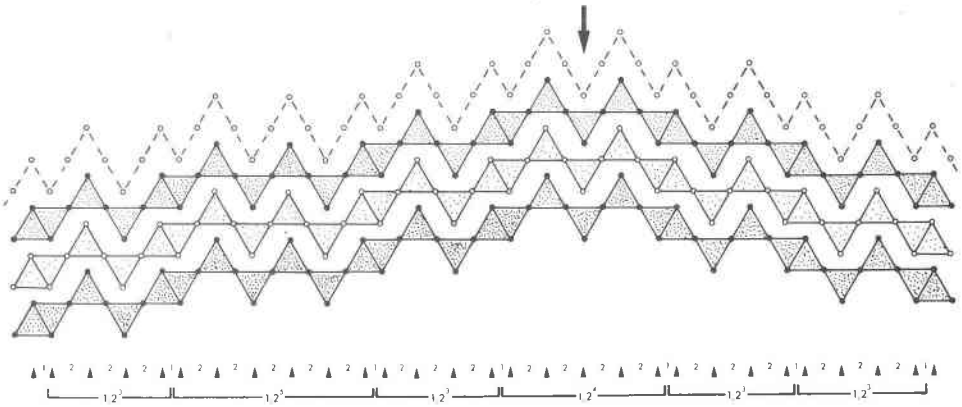

Fig. 14. Schematic [100] projection of trigonal prism sheets showing the insertion of a $(1, 2^4)$ band and a $(1, 2^5)$ band into a matrix of $(1, 2^3)$. Note that the former results in two regions of $(1, 2^3)$ leucophoenicite related by a mirror plane (twin boundary) while the latter does not. (Unit-cell twin planes are indicated by arrow heads; the "microscopic" twin plane by a heavy arrow.)

The decomposition of leucophoenicite to tephroite

The major difficulty experienced in this study of leucophoenicite was decomposition of the specimen in the electron beam. Under normal operating conditions, particularly for heavily faulted and/or micro-twinned crystals, damage resulted in the rapid and severe diminution of image contrast. Defocussing the beam allowed longer working times, but also necessitated longer (>20 second) photographic exposures, making high-resolution microscopy impossible. Slightly longer working times were available when the specimens were left in the microscope under vacuum overnight. This suggests that adsorbed water facilitates the reaction.

By removing the condenser aperture and focussing the beam, the decomposition was accelerated and tephroite, $(2)^2$, was produced. The reaction is presumably

$$Mn_7[SiO_4]_2[(SiO_4)(OH)_2] \rightarrow 3Mn_2SiO_4 + Mn(OH)_2.$$

Under the experimental conditions $Mn(OH)_2$ would probably further decompose to give MnO and H_2O, but only tephroite, Mn_2SiO_4, could be detected.

An example of a twinned leucophoenicite crystal and the tephroite decomposition product is shown in Figures 15a and b respectively; the micrographs are from precisely the same area. The tephroite consists of small domains, each apparently perfect in structure, but slightly misoriented with respect to adjacent domains. A higher-magnification image of this crystal (Fig. 16) suggests that the

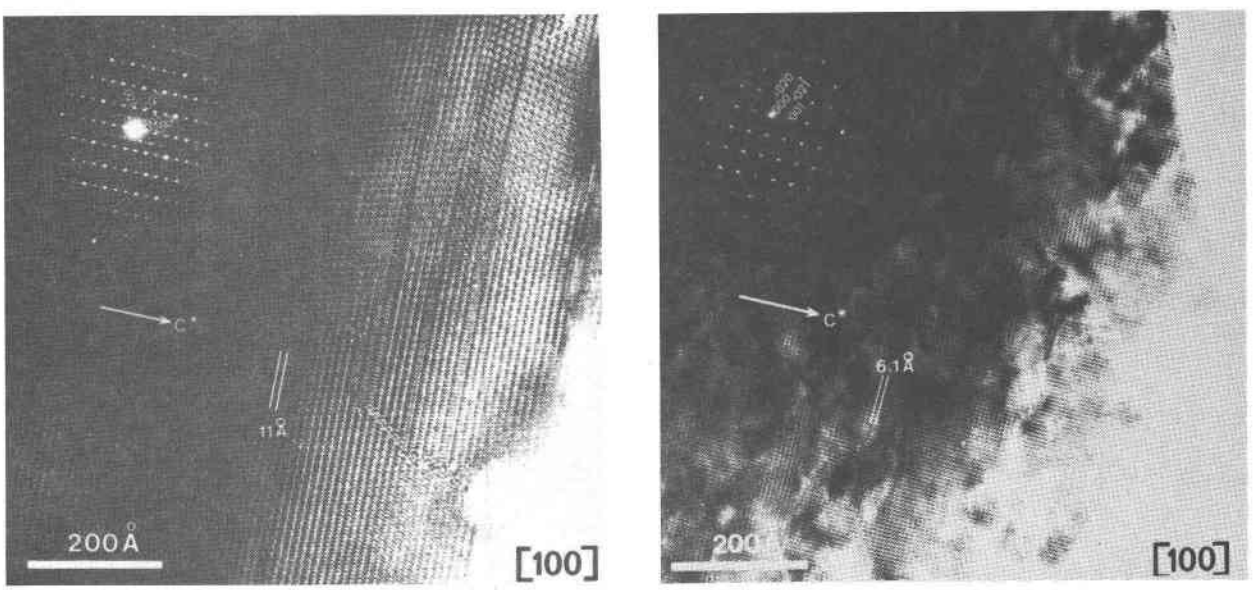

Fig. 15. A. A twinned $(1, 2^3)$ leucophoenicite crystal in the [100] projection direction (BM 1946, 185). B. The same crystal after it has been transformed to tephroite under the electron beam. Note the slightly mismatched domains.

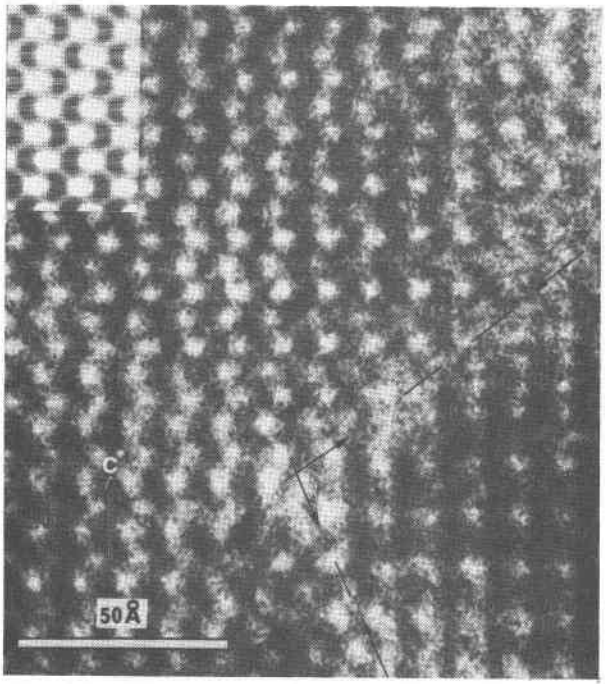

Fig. 16. A higher-magnification image of a domain boundary in Figure 15b (indicated by arrows). Also note the slight bending of the zig-zag rows of white dots on the left-hand side of the micrograph.

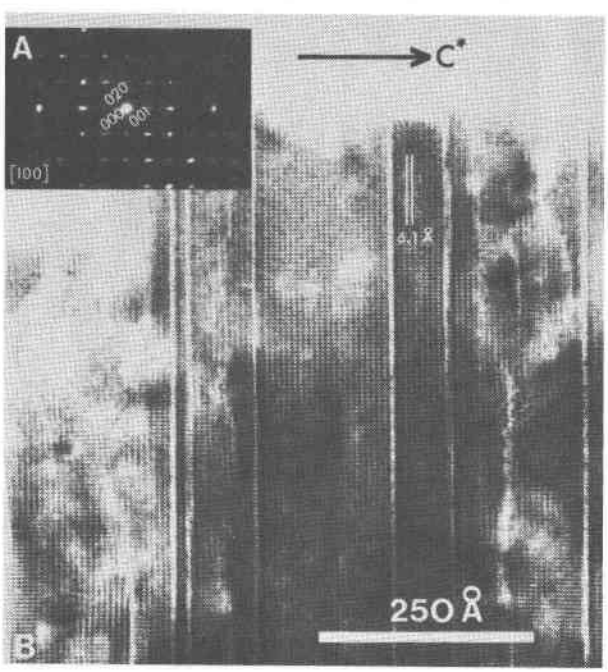

Fig. 17. A leucophoenicite crystal which has been incompletely transformed to tephroite. The lamellar faults are probably of the sort found in the alleghanyite minerals, *i.e.*, $Mn(OH)_2$ boundaries (BM 1946, 185).

domains are tilted with respect to the electron beam and/or that there is a variation in thickness across the transformed crystal.

Figure 17 shows an example of an incompletely transformed leucophoenicite crystal. In addition to the features already mentioned it contains a few lamellar faults which appear to be similar to those encountered in the alleghanyite (Mn-humite) series (White and Hyde, 1982b) *i.e.*, sellaite, $Mn(OH)_2$ layers (in Mn-norbergite lamellae).

X-ray powder diffraction

All three leucophoenicite specimens were poorly crystalline; they gave powder patterns with very broad reflections.

Moore's structural refinement of a Franklin specimen yielded the unit cell dimensions a = 4.826(6), b = 10.842(19), c = 11.324(9)Å, α = 103.93°(9). A typical Guinier camera powder pattern for our Franklin leucophoenicite (SI C6800) is given in Table 2. The refined unit cell parameters are a = 4.857(5), b = 10.82(2), c = 11.36(1)Å, α = 103.85°(12). Electron-probe microanalysis (EPMA) gave a cation ratio of Mn : Ca : Mg = 0.88 : 0.09 : 0.03 (+ trace Zn). The observed lines are in good agreement with previously published powder data

Table 2: Guinier powder data for leucophoenicite from Franklin, N.J. (SI C6800)

d(obs)	d(calc)	hkl	I/I_o
4.403	4.408	110	15
3.959	3.959	111	14
3.623	3.626	$1\bar{1}2$	22
3.288	3.286	112	18
2.969	2.975	$1\bar{1}3$	14
2.884	2.889	$1\bar{3}1$	69 b
2.755	2.758 2.752	004 $1\bar{3}2$	34
2.724	2.725 2.722	$0\bar{2}4$ 023	40
2.695	2.694	113	100
2.631	2.630	131	46
2.499	2.494	$1\bar{3}3$	14
2.451	2.452	$1\bar{1}4$	31
2.430	2.429	200	20
2.382	2.398 2.377	104 $1\bar{2}4$	23
2.366	2.366 2.363	210 $1\bar{4}1$	20
2.211	2.218 2.207	$2\bar{1}2$ 005	8
1.815	1.817 1.813	$0\bar{3}6$ $2\bar{2}4$	60 b
1.807	1.811 1.807 1.799	134 $\bar{2}41$ 232	31
1.577	1.577 1.576	161 007	17
1.567	1.566	$0\bar{6}5$	15

b broad lines

Table 3: Guinier powder data for leucophoenicite from Pajsberg, Sweden (SM 74024)

d(obs)	d(calc)	hkl	I/I_o
4.41	4.38	110	26
4.344			29
3.960	3.94	111	32
3.896			52
3.766			23
3.627	3.634 3.612	102 $1\bar{1}2$	26
3.566			35
3.423			26
3.284	3.281	112	56*
3.102			100
2.980	2.969	$1\bar{1}3$	23
2.881	2.881	$1\bar{3}1$	81 vb
2.831			42
2.755	2.766 2.745	004 $1\bar{3}2$	29
2.729	2.731 2.728	023 $0\bar{2}4$	74 b
2.691	2.694	113	74 b
2.626	2.628	131	26
2.453	2.451	$1\bar{1}4$	35
2.428	2.431 2.429	041 $0\bar{4}3$	26
2.375	2.374	$1\bar{2}4$	35
2.357	2.359	$1\bar{4}1$	26
2.324	2.323	$2\bar{1}1$	29
2.211	2.213 2.209 2.204	005 202 $2\bar{1}2$	94*
2.118	2.122	212	81*
2.106			65
2.057	2.059	$1\bar{1}5$	32
1.856			23
1.814	1.817 1.814	204 134	65 vb

b broad lines

*some intensity may be due to phases other than leucophoenicite

(Cook, 1969; Moore, 1970), although the relative intensities vary considerably between the three patterns.

The powder data for the Pajsberg (Sweden) specimen (SM 740214) are listed in Table 3. The refined unit cell parameters from the $(1,2^3)$ leucophoenicite reflections are a = 4.819(5), b = 10.82(1), c = 11.39(1)Å, α = 103.67°(22); EPMA gave a cation ratio of Mn : Ca : Mg : Ti : Al = 0.85 : 0.09 : 0.05 : 0.004 : 0.002. In agreement with Moore (1970) several additonal reflections were also present and, like Moore, we could attribute these to an orthorhombic unit cell with parameters similar to those of manganhumite (a = 4.870(4), b = 10.794(8), c = 22.61(1)Å); but selected area electron diffraction did not reveal the presence of this phase.

A major difference between the Swedish specimen and those from Franklin was the presence of chrysotile, $Mg_3Si_2O_5(OH)_4$ in the former. Analytical electron microscopy showed that the Mg was accommodated almost exclusively as chrysotile (which contained no Mn), whose characteristic filaments were intimately associated with platy leucophoenicite (Figs. 18 and 19). Although Mg made up only a very small proportion of the bulk analysis, the extreme morphology of chrysotile (fragments were a few hundred to 1000Å in diameter) resulted in very many chrysotile crystallites. (This effect was exaggerated in the EM work since the serpentine filaments remained in suspension longer than the larger leucophoenicite crystals, and were therefore selectively deposited upon the holey carbon films.) Attempts to correlate all the extra reflections on the powder patterns to known chrysotile unit cells were unsuccessful. A comparison of our electron diffraction patterns with those of Zussman *et al.* (1957) suggested that crystals were orthochrysotile or mixed ortho- and clino-polymorphs.

A leucophoenicite–manganhumite structural relationship

In Figure 2 the trigonal prism array of leucophoenicite is compared to that of manganhumite; the similarity between the structures is obvious. Figure 20 shows that if alternate lamellae, three trigonal prisms wide, in manganhumite are rotated 180° about an axis at $x = \pm 1/4$ along the trigonal prism edges parallel to **c***, the $(1,2^2,1,2^4)$array

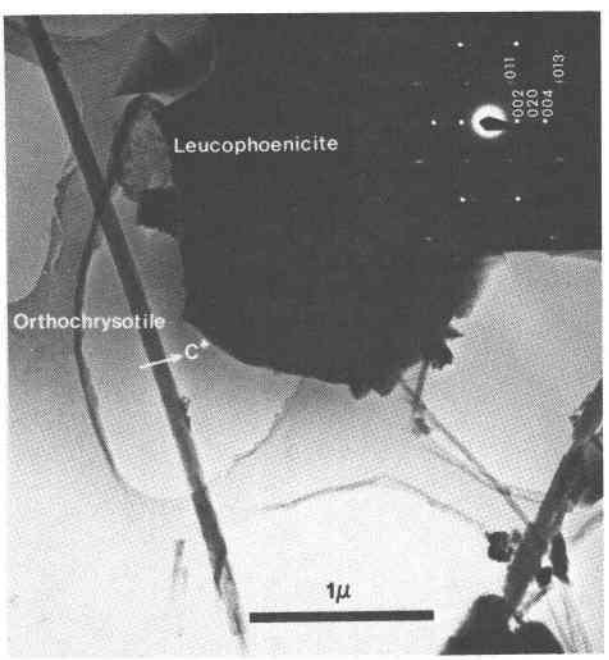

Fig. 18. An electron diffraction pattern and low-magnification image of chrysotile (SM 740214). The diffraction pattern indexing is for orthochrysotile according to Zussman *et al.* (1957), but additional spots indicate that clino-chrysotile is also present. Note that the serpentine crystal is not thick enough to obscure the underlying carbon film. Also present is a large, platy leucophoenicite crystal.

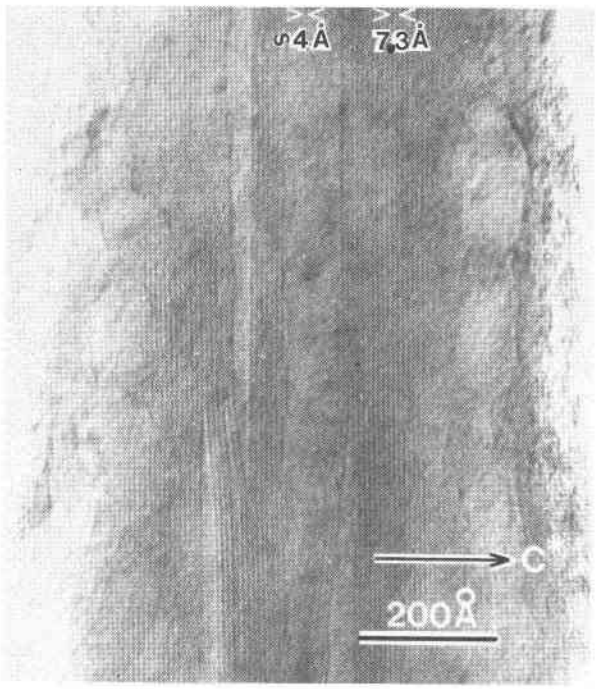

Fig. 19. A higher resolution image of an orthochrysotile filament. The ~7.3Å fringes correspond to $d(002)$; the ~4Å central fringes are probably $d(020)$. (The relevant unit cell parameters are: a = 5.322, b = 9.219, c = 14.53Å for orthochrysotile.)

is obtained. A translation of alternate $(1,2^2,1,2^4)$ blocks by **a**/2 then yields $(1,2^3)$ leucophoenicite. Hence there is a simple, direct "unit-cell twinning" relation between the two structures (in addition to the crystallographic shear relationship previously noted (White and Hyde, 1983)).

Humite-like boundaries [*i.e.*, twinned c.c.p. (3) bands] were observed in leucophoenicite, but only rarely. An example is given in Figures 21 and 22. The $\mathbf{Re_3B}$ portion of the manganhumite region is a *single* thin lamella (white in the image, due to its lower charge density). All other white lamellae occur as *consecutive pairs* which are characteristic of the statistical distribution of Si over the face-sharing trigonal prismatic (edge-sharing tetrahedral) sites through the thickness of the crystal. The result is an average charge density over these interstices which is half that of the adjacent olivine portions, whose trigonal prisms are fully occupied by Si. The boundary is shown schematically in Figure 22b. Note that neither the manganhumite portion nor the $(1,2^4)$ lamellae (because these always occur in pairs) introduce a microtwin into the $(1, 2^3)$ leucophoenicite. This is borne out by the electron diffraction pattern which shows no doubling of the number of spots in the $(13l)$ row.

Conclusion

Previous studies of leucophoenicite yielded interesting though perplexing results. In particular, the additional orthorhombic reflections in X-ray powder diffraction patterns could not be explained. Our work is similarly inconclusive; both HREM and SAD failed to elucidate the origin of the apparent orthorhombic symmetry. Moore (1970) suggested that the extra reflections could be due to polysynthetic twinning on a unit cell scale but although we find frequent twinning (on a scale of less than 100Å) it is not periodic. Superlattices were not detected, although partly ordered intergrowths were observed (Figs. 7, 9 and 21). (In the related humites regular intergrowth sometimes occurs, yielding long c-axes (White and Hyde, 1982a,b).)

Moore (1967) also reported that Weissenberg photographs for some leucophoenicite specimens showed streaking parallel to **c***. This he attributed to "semi-random structure." Some of our electron diffraction patterns were similarly streaked, and this was seen to be due to coherent intergrowth of various leucophoenicite-like structures $(1,2^x, x > 3)$—a phenomenon observed in all the specimens used in this study. (It is interesting that $(1,2^x)$ structures with $x < 3$ were never seen.)

Complex faulting occurs extensively in one specimen

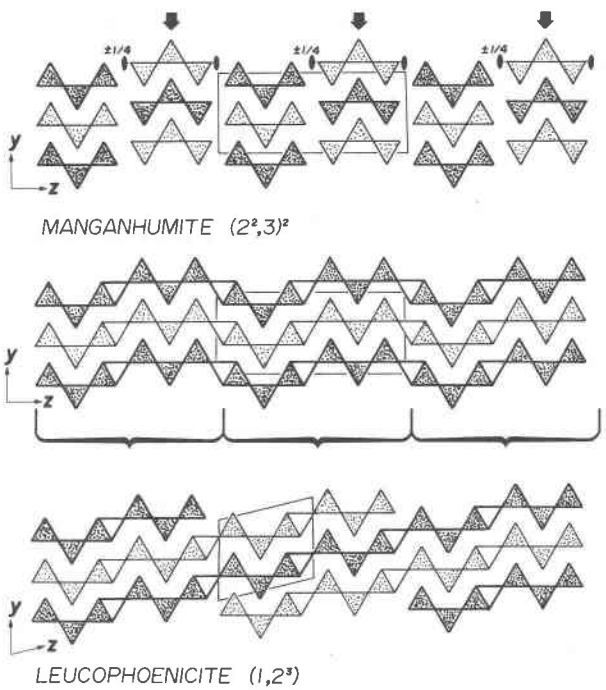

Fig. 20. A schematic drawing of the way in which manganhumite may be structurally related to leucophoenicite. A. The manganhumite structure, $(2^3, 3)^2$ projected on (100). B. The structure obtained by rotating alternate lamellae of trigonal prisms of width $d(002)$ in manganhumite about an axis at $x = \pm 1/4$ has a unit cell equivalent to that of manganhumite. The new trigonal prisms produced by the operation are left unshaded. The twin formula is $(1, 2^2, 1, 2^4)$. C. The leucophoenicite structure $(1, 2^3)$ is formed by translating alternate $(1, 2^2, 1, 2^4)$ blocks through **a**/2.

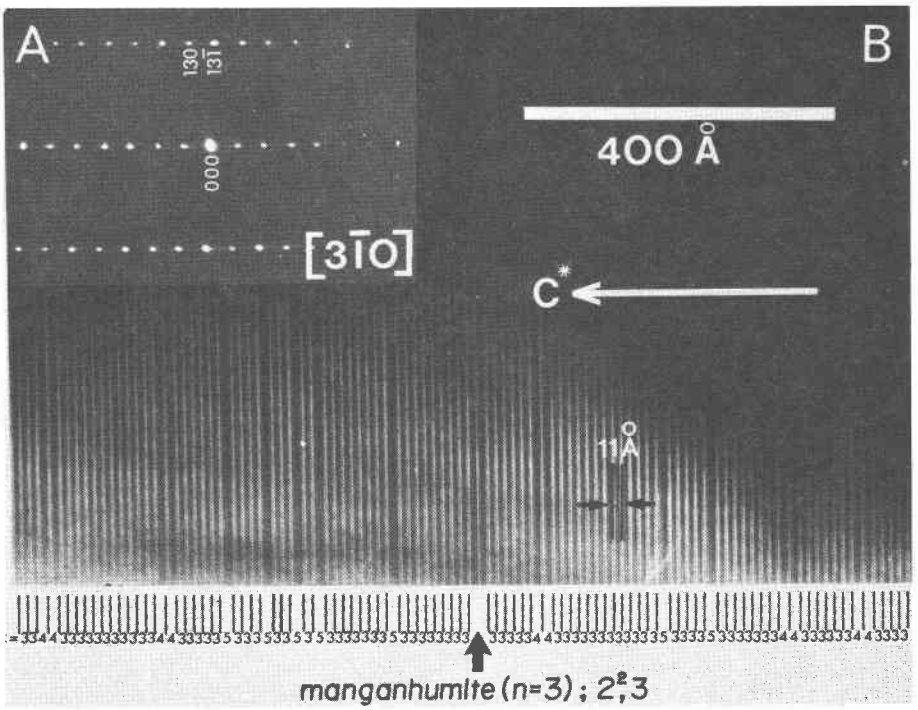

Fig. 21. A disordered leucophoenicite crystal (BM 1946, 185). A. SAD pattern. B. Low magnification micrograph showing the extent of disorder in the crystal. Variations in lattice spacing have been interpreted as mainly (1, 2^x) members; but a thin lamella of manganhumite is also present.

(BM 1946, 185; Figs. 10 and 15a). Similar faults observed in the humite series (White and Hyde, 1982b) were rather rare, not nearly as common as in leucophoenicite. Microtwinning was also less frequent in the humites than in leucophoenicite.

The apparently statistical distribution of Si between O_4 tetrahedra in edge-sharing pairs (*i.e.*, in face-sharing trigonal prisms of cations) was a little surprising; at least some short-range order was expected. Naturally, in terms of the number of unit cells the specimens examined were quite thick: $8.5 \times a \simeq 40$Å and $4 \times b \simeq 40$Å in the micrographs shown in Figures 5 and 6 respectively. The possibility of ordering in the [100] direction was considered, but rejected because it would result in a doubled *a*-axis for which there was no evidence in any X-ray or electron diffraction pattern. Furthermore, comparison of observed and computer-simulated images in the [010] zone, which would reveal ordering along **a**, instead showed good agreement with the "statistical model."

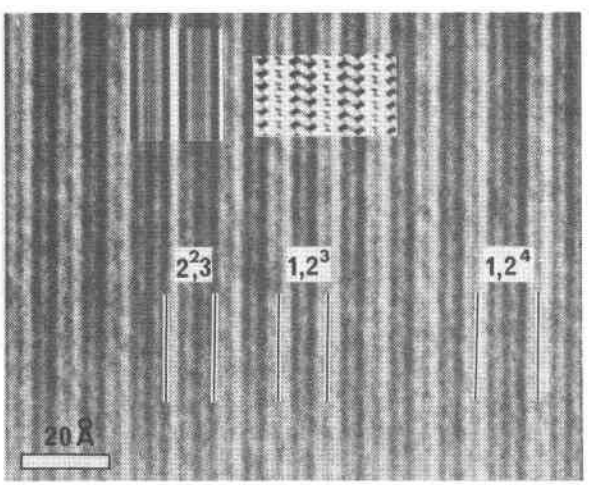

A

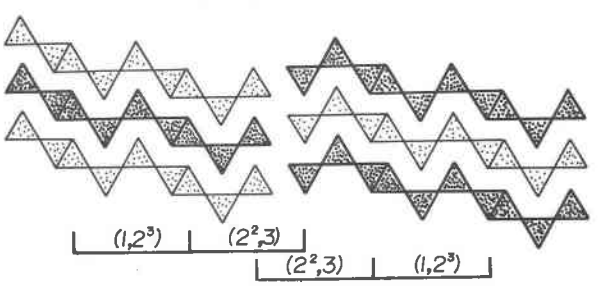

B

Fig. 22. A. An enlargement of the manganhumite region in Figure 21. Images were calculated for manganhumite and for (1, 2^3) leucophoenicite. B. A schematic illustration of the boundary.

(Nevertheless, the possibility of electron beam effects inducing disorder in ordered leucophoenicite samples should not be discounted.)

Acknowledgments

The authors are grateful to Mr. P. C. Tandy (British Museum, Natural History), Mr. Pete J. Dunn (Smithsonian Institution) and Dr. B. Lindqvist (Swedish Museum of Natural History) for providing leucophoenicite specimens. We are also indebted to Dr. J. R. Sellar and Dr. R. A. Eggleton for preparing the image calculation program, Mr. N. Ware for carrying out electron probe analyses of the samples, Dr. D. Goodchild for the use of an analytical TEM, and Dr. Joyce Wilkie for the preparation of petrographic thin sections and providing the computer program for refining Guinier powder data. Many useful discussions with Dr. E. Makovicky clarified several problems in the early stages of this work. T. J. White acknowledges the financial assistance provided by the Commonwealth Department of Education and the A.N.U.

References

Cook, D. (1969) Leucophoenicite, alleghanyite and sonolite from Franklin and Sterling Hill, New Jersey. American Mineralogist, 58, 807–824.

Hyde, B. G., Andersson, S., Bakker, M., Plug, C. M., and O'Keeffe, M. (1979) The (twin) composition plane as an extended defect and structure-building entity in crystals. Progress in Solid State Chemistry, 12, 273–327.

Moore, P. B. (1967) On leucophoenicites: I A note on form developments. American Mineralogist, 52, 1226–1232.

Moore, P. B. (1970) Edge-sharing silicate tetrahedra in the crystal structure of leucophoenicite. American Mineralogist, 55, 1146–1166.

Palache, C. (1928) Mineralogical notes on Franklin and Sterling Hill, New Jersey. American Mineralogist, 13, 297–329.

White, T. J. and Hyde, B. G. (1983) A description of the leucophoenicite family of structures and its relation to the humite family. Acta Crystallographica, B39, 10–17.

White, T. J. and Hyde, B. G. (1982a) An electron microscope study of the humite minerals: I Mg-humites. Physics and Chemistry of Minerals, 8, 55–63.

White, T. J. and Hyde, B. G. (1982b) An electron microscope study of the humite minerals: II Mn-humites. Physics and Chemistry of Minerals, 8, 167–174.

Zussman, J., Brindley, G. W. and Comer, J. J. (1957) Electron diffraction studies of serpentine minerals. American Mineralogist, 42, 133–153.

Manuscript received, May 26, 1982;
accepted for publication, February 10, 1983.